Surface-plasmon fields in two-dimensional arrays of gold nanodisks*

W. L. Johnson[a], S. A. Kim[a], Z. N. Utegulov[b], and B. T. Draine[c]

[a]Materials Reliability Division, National Institute of Standards and Technology, 325 Broadway, Boulder CO 80305 [b]Department of Chemistry, University of Nebraska, Lincoln, Nebraska 68588
[c] Department of Astrophysical Sciences, Princeton University, Princeton, NJ, USA 08544

ABSTRACT

Distributions of electric fields in two-dimensional arrays of gold nanodisks on Si_3N_4 membranes are modeled by use of the discrete-dipole approximation as a function of nanodisk diameter (20 nm to 50 nm), height (10 nm to 100 nm), ratio of the array spacing to diameter (1.3 to 4.7), and angle of incident light. The primary focus is on fields in a plane near the circular gold/vacuum interface with light of 532 nm wavelength incident through the membrane, a configuration that is particularly relevant to potential applications in plasmon-mediated Brillouin light scattering, nanolithography, and photovoltaics. The height/diameter ratio for maximum intensities over this plane is between 0.7 and 1.5 and not strongly dependent on the spacing for a given angle. The average intensity increases with decreasing array spacing and incident angle relative to the substrate normal. This dependence is attributed primarily to a combination of fractional coverage area of the gold and increased excitation of a dipolar contribution to the fields. The incident light at 532 nm simultaneously excites dipolar and quadrupolar surface-plasmon modes. Because the quadrupolar mode has a peak close to 532 nm, its excited fields are approximately out of phase with the incident light.

Keywords: Brillouin light scattering, dipole resonance, discrete-dipole approximation, electric fields, nanodisk arrays, quadrupole resonance, surface plasmons

1. INTRODUCTION

Surface plasmons excited by incident monochromatic light in arrays of noble-metal nanodots have been a subject of much interest in recent years because of potential applications in surface-enhanced spectroscopy[1–5], nanolithography,[6,7] integrated-circuit waveguides,[8–12] and photovoltaics.[13–17] Electric fields in such structures depend on numerous parameters, including target geometry, material properties, and wavevector of incident light that excites the surface plasmons. Only a fraction of this parameter space has been explored thus far, although numerous papers have been published on this subject.[2,6,8,12,18–29] Because complete field calculations are computationally intensive, most modeling studies have been restricted to normal-incidence far-field extinction, absorption, or scattering, which are less time-consuming to model than near fields.

In this report, we present calculations of electric-field intensities in two-dimensionally periodic square arrays of gold nanodisks on Si_3N_4 membranes as a function of nanodisk diameter (20 nm to 50 nm), nanodisk height (10 nm to 100 nm), ratio of array spacing to diameter (1.3 to 4.7), and angle of incident light. The primary focus is on field intensities in vacuum near the circular surface of the nanodisks, with 532 nm light incident on the opposite Si_3N_4 surface. In other words, we are interested in intensities in a plane near the flat surfaces of the nanodisks facing away from the incident light. This orientation of the incident wavevector differs from that in most previous studies of surface plasmons in nanodot (disk, spherical, or pyramidal) arrays, which have generally considered light incident directly on the surfaces of nanodots supported by a substrate or surrounded by homogeneous dielectric material or vacuum.

Further author information: (Send correspondence to Ward L. Johnson)
E-mail: wjohnson@boulder.nist.gov, Telephone: 303-497-5805

Plasmonics: Metallic Nanostructures and Their Optical Properties VI, edited by Mark I. Stockman
Proc. of SPIE Vol. 7032, 70321S, (2008) · 0277-786X/08/$18 · doi: 10.1117/12.795608

Our principal motivation for studying a scattering geometry that is inverted relative to previous studies is an interest in optimizing field-intensity distributions of surface plasmons in nanodisk arrays that mediate Brillouin scattering of photons by phonons in a specimen brought within a few nanometers of the array. As proposed by Utegulov *et al.*,[30] nanometer-scale variations of surface-plasmon fields in a gold or silver nanodisk array may enable detection of phonons with wavenumbers beyond the limits of conventional Brillouin light scattering (BLS) through band folding in the plasmonic crystal that is formed by the array. The inverted scattering geometry is also relevant to potential applications of surface-plasmon field enhancement in photovoltaics and nanolithography.

Membranes with nanoscale thickness were selected in this study as substrates for the nanodisks, because these provide volumes of the unit cells of the arrays that are small enough to enable practical computation times. The particular choice of Si_3N_4 arises from the fact that membranes of this material are readily available commercially and, therefore, feasible to employ in future experiments. The choice of a wavelength of 532 nm as a primary focus arises from the fact that this is a typical wavelength employed in BLS systems.

We find that the nanodisk height/diameter ratio that provides maximum field intensities near the circular gold/vacuum interface is on the order of unity and not strongly dependent on array spacing for a given angle of incidence. The average intensity over a plane 2 nm from the circular Au/vacuum interface increases with decreasing array spacing and incident angle relative to the substrate normal, for angles between 0° and 40°. Several factors contribute to this dependence, including fractional coverage area of the gold, changes in field symmetry with angle, and relative strengths of contributions from two normal modes.

2. METHODS

The coordinate system, orientation of the incident wavevector, and dimensional parameters of a unit cell of the array are defined in Fig. 1. The gold nanodisk is a solid cylinder with diameter d and height h. The array is periodic in y and z with a spacing Λ in both directions. The thickness of the Si_3N_4 substrate is 50 nm. The wavevector $\vec{k}_0$ and polarization of the incident light lie in the x-y plane, and the wavelength ($2\pi/|\vec{k}_0|$) of this light is 532 nm, except where otherwise noted (in absorption spectra).

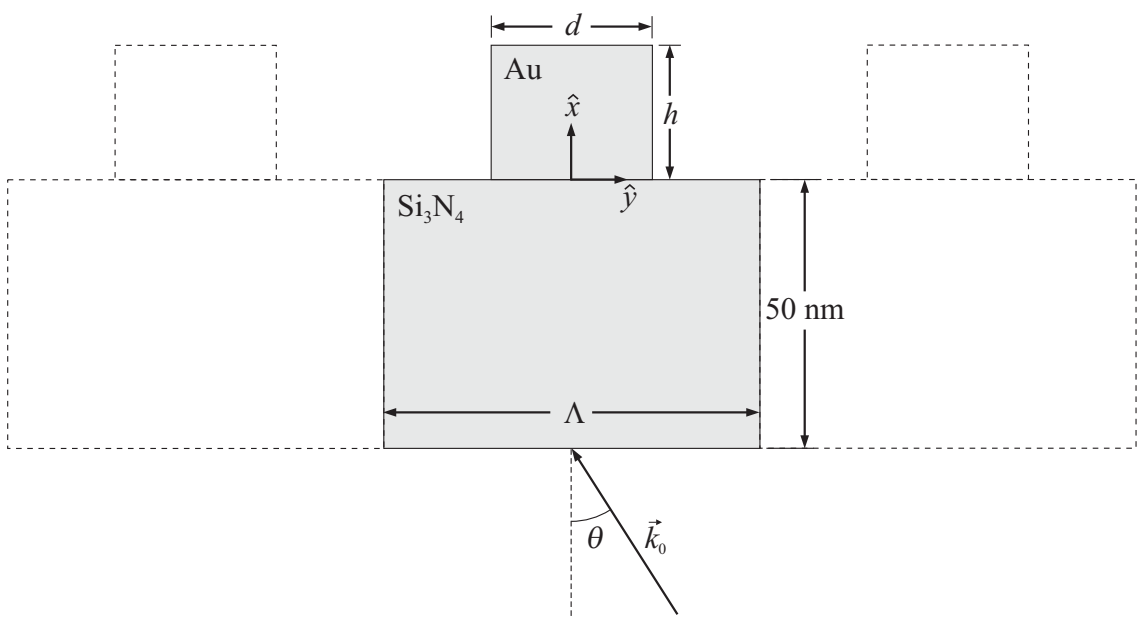

Figure 1. Cross-sectional geometry of the unit cell and definitions of axes and dimensional parameters. Dashed lines indicate adjacent unit cells. The origin ($x = y = z = 0$) of the coordinate system is at the center of the bottom circular surface (Au/Si_3N_4 interface) of one of the nanodisks.

We have employed the discrete dipole approximation[31–33] to calculate the electromagnetic fields within periodic targets with the unit cell of the array having the geometry shown in Fig. 1. The calculations were carried

out with version 7.0.1 of the open-source code DDSCAT.[34,35] As input to the calculations, the complex index of refraction of gold as a function of wavelength was taken to be that measured by Johnson and Christy[36] for an evaporated gold film. The real part n of the index of refraction of Si_3N_4 was taken from the experimental results of Philipp.[37] Since Philipp does not report values of the imaginary part k of the index of refraction of Si_3N_4 in the range of wavelengths of interest here, values of k were taken from the modified Lorentz-oscillator model of Djurišić and Li,[38] which was fit to Philipp's[37] data at shorter wavelengths. At 532 nm, the indices of refraction were $n = 0.544$ and $k = 2.231$ for gold and $n = 2.036$ and $k = 0.016$ for Si_3N_4.

Since surface-plasmon fields vary significantly on a single-nanometer scale, discrete-dipole calculations ideally should be performed with a dipole-grid spacing of ∼1 nm or less. However, considering the relatively wide range of parameter space explored in this study, the computation time that would be involved in such calculations is prohibitive. Our calculations were performed with a grid spacing of 5 nm. This spacing is sufficient for the purpose of this study, which is to determine the form and trends in the intensity distributions as a function of geometric parameters. A limited number of additional calculations with a spacings of 2.5 nm were performed (as indicated below) to confirm results obtained with the larger spacing and to reduce visible artifacts in field plots arising from the discrete grid.

3. RESULTS

Figure 2 shows an example of electric-field intensities $|E|^2$ within the unit cell relative to the intensity $|E_0|^2$ of the incident light for an array with $d = 30$ nm, $h = 30$ nm, $\Lambda = 60$ nm, and $\theta = 40°$. The intensities in Fig. 2(a) are over the x-y plane ($z = 0$), and those in Fig. 2(b) are over a surface perpendicular to the substrate normal and 2 nm above the disk (denoted as surface I).

As indicated above, our central focus is electric-field intensities over surface I. Fig. 3 shows calculations of average intensity $(|E|^2/|E_0|^2)_{avg}$ and maximum intensity $(|E|^2/|E_0|^2)_{max}$ over this surface with $d = 30$ nm, $\theta = 60°$, h from 10 nm to 100 nm, and Λ from 60 nm to 140 nm. The value of h at which intensities are greatest depends only weakly on Λ. Corresponding values of the aspect ratio $(h/d)_{peak}$ at which intensities are greatest (determined from a polynomial fit of points near the peaks) are plotted versus Λ/d in Fig. 4, along with results for $\theta = 60°$ with $d = 30$ nm and $\theta = 0°$, 30°, and 60° with $d = 50$ nm. With the exception of normal incidence ($\theta = 0°$), all of these curves show similar weak dependence of $(h/d)_{peak}$ on Λ. Values of $(h/d)_{peak}$ are, in each case, between 0.7 and 1.5.

To further explore the dependence of $(|E|^2/|E_0|^2)_{avg}$ and $(|E|^2/|E_0|^2)_{max}$ on Λ/d and θ, we proceed by fixing the value of h/d at 1. Fig. 5 shows plots of $(|E|^2/|E_0|^2)_{avg}$ and $(|E|^2/|E_0|^2)_{max}$ as a function of Λ/d with θ from 0° to 60° for nanodisks with a diameter of 30 nm. With the exception of $\theta = 60°$, $(|E|^2/|E_0|^2)_{avg}$ increases systematically with decreasing Λ/d and θ in the calculated range.

A simple geometric factor contributes to the increase in $(|E|^2/|E_0|^2)_{avg}$ with decreasing Λ (Fig. 5). If the highest intensities occur within a few nanometers of the surface of the nanodisk and these remain approximately constant, $(|E|^2/|E_0|^2)_{avg}$ will increase as the ratio of the circular surface area of the gold to the area of the unit cell (Λ^2) increases.

Another relatively simple factor contributes to the variations in $(|E|^2/|E_0|^2)_{max}$ at the larger values of Λ and nonzero θ. As Λ is increased, the edge of the disk near the most intense region on surface I (the right edge in Fig. 2(b)) is less shaded from the incident light by the adjacent disk, leading to an enhanced "lightning rod" effect at this edge and correspondingly higher intensities.

Changes in intensity distributions that occur with decreasing Λ and θ are illustrated by the differences of Fig. 6 (with $\Lambda = 40$ nm and $\theta = 0°$) relative to Fig. 2 (with $\Lambda = 60$ nm and $\theta = 40°$). As Λ and θ are reduced, $(|E|^2/|E_0|^2)_{avg}$ over surface I (Fig. 6(b)) increases (as shown also in Fig. 5). This is associated partly with an increase in intensity near the left edge of the disk, in addition to the geometric effect mentioned above. In this case, there is relatively little change in $(|E|^2/|E_0|^2)_{max}$ on surface I, which occurs near the right edge of the disk in Figs. 2(b) and 6(b). Similar trends of intensity distributions as a function of Λ and θ are found in arrays of disks with $d = 50$ nm (not shown).

Insight into the nature of the surface-plasmon modes that contribute to the fields is provided by the spectra of absorption (fraction of incident energy not transmitted or scattered) that are plotted in Fig. 7 for the same

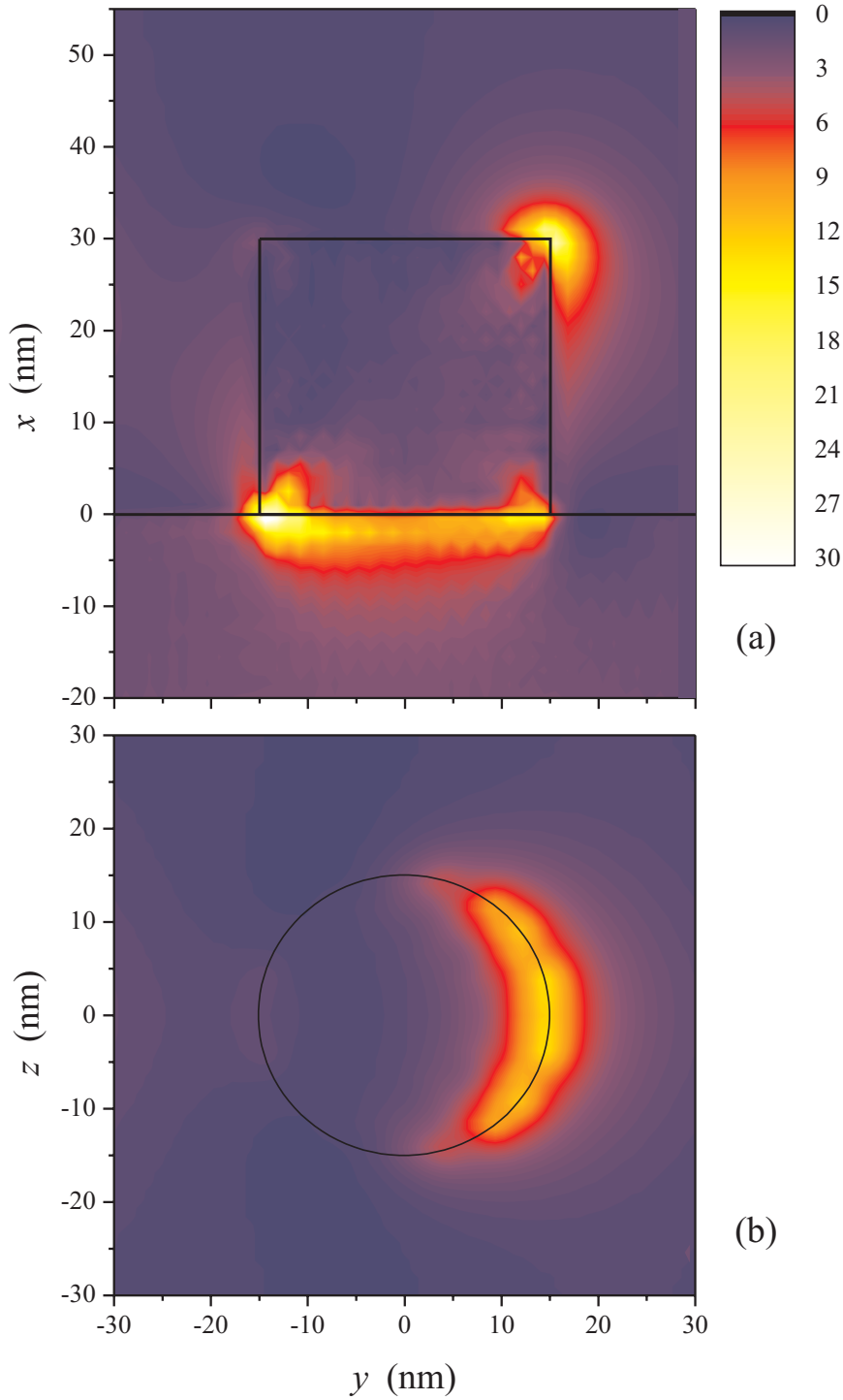

Figure 2. Relative electric-field intensities $|E|^2/|E_0|^2$ over (a) the x-y plane ($z = 0$) and (b) surface I with $d = 30$ nm, $h = 30$ nm, $\Lambda = 60$ nm, and $\theta = 40°$. DDSCAT dipole spacing = 2.5 nm.

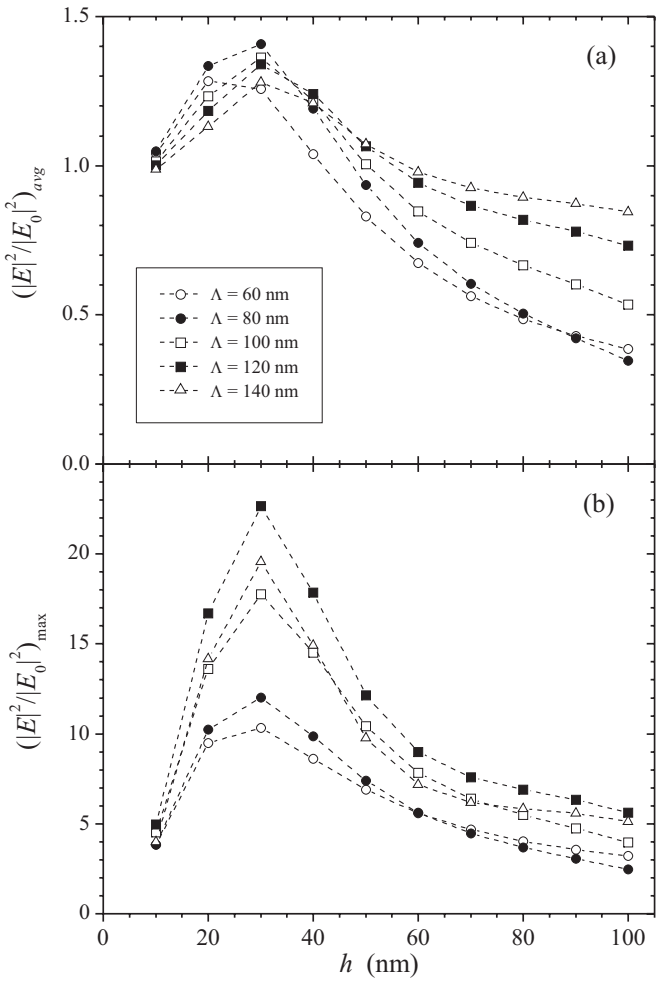

Figure 3. (a) Average intensity $(|E|^2/|E_0|^2)_{avg}$ and (b) maximum intensity $(|E|^2/|E_0|^2)_{max}$ over surface I as a function of h with $d = 30$ nm, $\theta = 60°$, and $\Lambda = 60$ nm to 140 nm.

values of d, θ, and Λ as those of Figs. 2 and 6. The absorption peak near 570 nm arises from resonant excitation of the "dipolar" surface-plasmon mode, which has been previously predicted and measured for a variety of gold and silver nanodot array geometries.[18–29] The field distributions of this mode are not necessarily very similar to a simple dipole, because of the lowering of symmetry that arises from the presence of the substrate and nonzero wavevector (when θ is nonzero). As reflected in published extinction spectra, the position of the dipole peak in two-dimensional arrays first blue shifts with decreasing spacing and, then, red shifts as interparticle coupling becomes more significant.[19,20,25,26] The peak on the lower-wavelength side of the dipole resonance is understood to arise from a "quadrupolar" surface-plasmon resonance.[18,19,23,25–28] This peak appears in Fig. 7 in the range of 520 nm to 535 nm, closely matching the wavelength of 532 nm that is used in the calculations of Figs. 2-6.

The response of a normal mode is 90° out-of-phase with an excitation when the mode is driven at its resonant frequency.[39] Therefore, with 532 nm incident light, the coincidence of the frequency of the quadrupole mode being close to the excitation frequency leads to electric fields from this mode being essentially 90° out-of-phase with that of the incident light. On the other hand, because such incident light is at a frequency higher than that of the dipole mode, the fields from the dipole mode are expected to have a phase between 90° and 180° relative to the excitation (contributing to both in-phase and out-of-phase fields). The symmetries of the in-phase and out-of-phase components of the electric-field vectors (not shown) for the configuration of Fig. 6 (with $\theta = 0$) are consistent with this expectation. Those for the oblique-incidence configuration of Fig. 2 have a

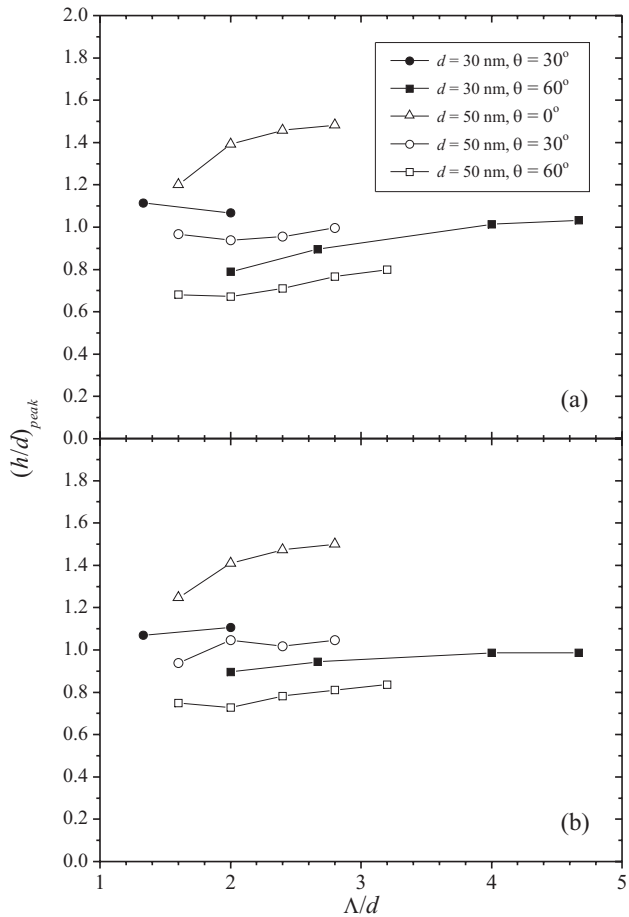

Figure 4. Aspect ratio $(h/d)_{peak}$ that provides the highest (a) $(|E|^2/|E_0|^2)_{avg}$ and (b) $(|E|^2/|E_0|^2)_{max}$ on surface I, plotted as a function of Λ/d for 30 nm and 50 nm nanodisks at several values of θ.

less obvious correspondence to dipole-like and quadrupole-like symmetry, because finite θ eliminates one of the vertical reflection planes.

The heights of the peaks in the two curves in Fig. 7 suggest that the strength of the quadrupole excitation increases relative to that of the dipole excitation at lower θ and Λ. Corresponding to this, one might assume that the magnitude of the out-of-phase component of the fields increases and that this contributes to the relative increase in $(|E|^2/|E_0|^2)_{avg}$ that is calculated for surface I (Fig. 5). This turns out to be an incorrect assumption. The increase in $(|E|^2/|E_0|^2)_{avg}$ of the fields in Fig. 6(b) relative to that of Fig. 2(b) is found to arise primarily from an increase in the in-phase (dipole) component of the electric field. Note that $(|E|^2/|E_0|^2)_{avg}$ is calculated only for surface I and, therefore, is not a measure of the average field intensities over the entire unit cell. The subject of the symmetries of the normal modes and the corresponding in-phase and out-of-phase field contributions will be considered further in a subsequent paper.

The broad background of the absorption at wavelengths below the peaks in Fig. 7 is understood to arise primarily from interband transitions in the gold, as reflected in the index of refraction.[36] Consistent with this intepretation, we find that this background is not significantly affected by reducing the imaginary part of the index of refraction k of Si_3N_4 to zero in the calculations (eliminating the contribution of Si_3N_4 to the absorption). For example, at 400 nm, the change in absorption arising from this change in the value of k of Si_3N_4 is only 2.6 %.

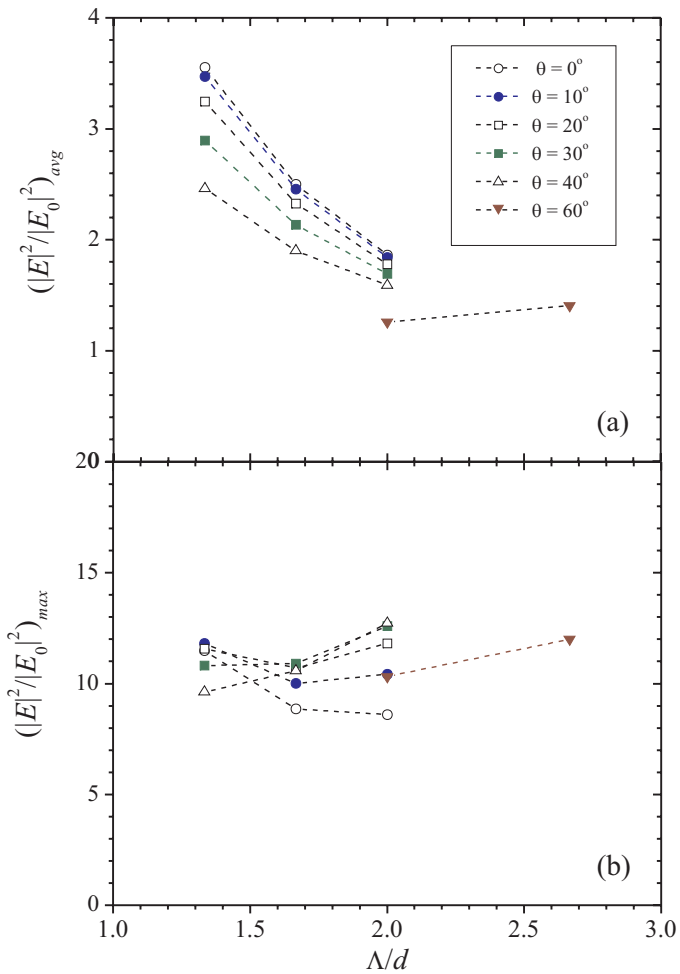

Figure 5. (a) Average intensity $(|E|^2/|E_0|^2)_{avg}$ and (b) maximum intensity $(|E|^2/|E_0|^2)_{max}$ over surface I as a function of Λ/d with $d = 30$ nm, $h = 30$ nm, and $\theta = 0°$ to $60°$.

4. CONCLUSION

In this modeling study, we have found that the aspect ratio h/d for optimal average and maximum intensities, $(|E|^2/|E_0|^2)_{avg}$ and $(|E|^2/|E_0|^2)_{max}$, over a surface (surface I) near the circular nanodisk/vacuum interface facing away from the incident 532 nm light (with light incident through the substrate) is not strongly dependent on nanodisk spacing Λ for a given incident angle θ over the ranges studied. The optimal values of h/d are between 0.7 and 1.5 for the range of parameters studied. With fixed h/d and θ in the range of 0° to 40°, $(|E|^2/|E_0|^2)_{avg}$ increases monotonically with decreasing Λ and θ. This behavior is attributed partly to the geometric effect of fractional coverage area of the gold and partly to enhanced field intensities near the edge of the disk away from the incident light (the left edge of the disk in Figs. 2(b) and 6(b)).

At 532 nm, "dipolar" and "quadupolar" extended surface-plasmon modes are simultaneously excited. This leads to in-phase and out-of-phase components of the fields with correspondingly different symmetries. The in-phase (dipole) contribution to the fields over surface I increases with decreasing Λ and θ.

With respect to the feasibility of implementing surface-enhanced BLS, the calculations presented here are encouraging. They indicate that significant average normalized intensities ($(|E|^2/|E_0|^2)_{avg}$ greater than 3) are achievable over the surface of a specimen brought within a few nanometers of nanodisk arrays that have values of Λ an order of magnitude smaller than the wavelength of the incident light. Since nanoscale variations of

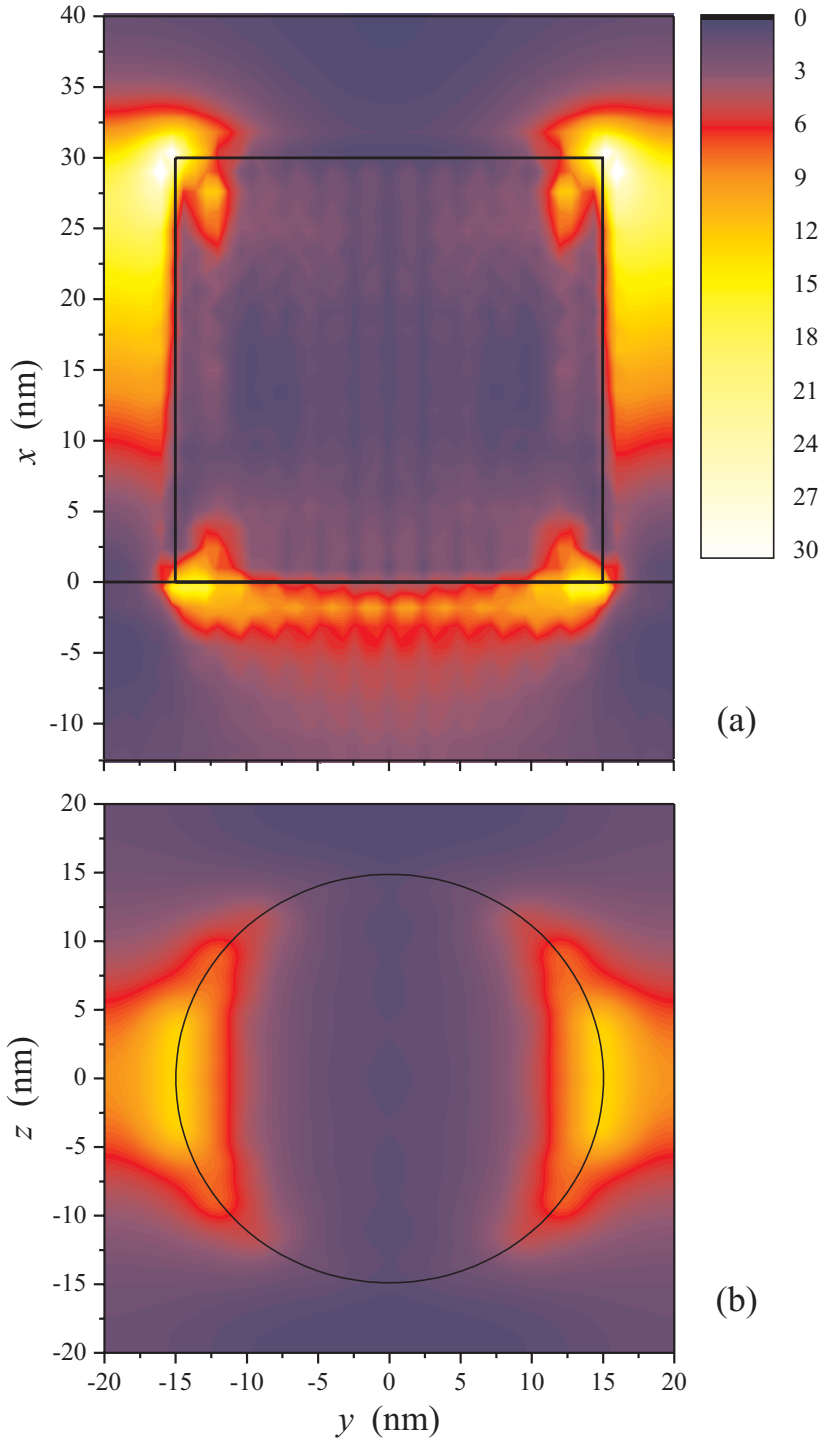

Figure 6. Relative electric-field intensities $|E|^2/|E_0|^2$ over surface I with $d = 30$ nm, $h = 30$ nm, $\Lambda = 40$ nm, and $\theta = 0°$. DDSCAT dipole spacing = 2.5 nm.

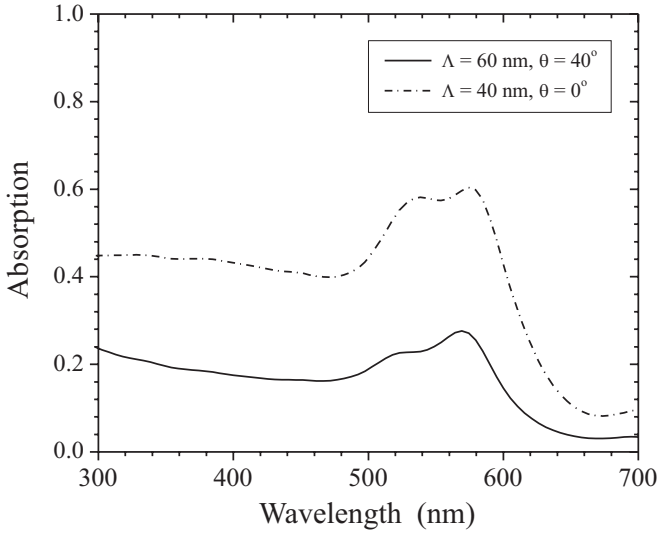

Figure 7. Absorption (fraction of energy not transmitted or scattered) of nanodisk arrays with $d = 30$ nm and $h = 30$ nm.

fields over the unit cell correspond to spatial Fourier components with correspondingly small wavelengths, the results support the suggestion of Utegulov *et al.*[30] that surface-plasmon mediation may enable practical BLS from phonons with wavelengths in the range of tens of nanometers. The predicted dependence of the intensity patterns on θ is also noteworthy. It suggests the possibility of varying θ to manipulate intensity distributions and selectively couple to phonons with prescribed wavelengths in a manner operationally similar to conventional BLS.

REFERENCES

[1] Gunnarsson, L., Bjerneld, E.J., Xu, H., Petronis, S., Kasemo, B., and Kall, M., "Interparticle coupling effects in nanofabricated substrates for surface-enhanced Raman scattering," *Appl. Phys. Lett.*, *78(6)*, 802 (2001).

[2] Félidj, N., Aubard, J., Levi, G., Krenn, J. R., Hohenau, A., Schider, G., Leitner A., and Aussenegg, F. R., "Optimized surface-enhanced Raman scattering on gold nanoparticle arrays," *Appl. Phys. Lett.*, *82*, 3095 (2003).

[3] De Jesús, M. A., Giesfeldt, K. S., Oran, J. M., Abu-Hatab, N. A., Lavrik, N. V., and Sepaniak, M. J., "Nanofabrication of densely packed metal-polymer arrays for surface-enhanced Raman spectrometry," *Appl. Spectrosc.*, *59*, 1501 (2005).

[4] Grand, J., de la Chapelle, M. L., Bijeon, J.-L., Adam, P.-M., Vial, A., and Royer, P., "Role of localized surface plasmons in surface-enhanced Raman scattering of shape-controlled metallic particles in regular arrays," *Phys. Rev. B*, *72(3)*, 33407 (2005).

[5] Yu, Q., Guan, P., Qin, D., Golden, G., and Wallace, P. M., "Inverted size-dependence of surface-enhanced Raman scattering on gold nanohole and nanodisk arrays," *Nano Lett.*, *8*, 1923 (2008).

[6] Koenderink, A. F., Hernández, J. V., Robicheaux, F., Noordam, L. D., and Polman, A., "Programmable nanolithography with plasmon nanoparticle arrays," *Nano Lett.*, *7*, 745 (2007).

[7] Kik, P. G., Martin, A. L., Maier, S. A., and Atwater, H. A.,"Metal nanoparticle arrays for near field optical lithography," *Proc. SPIE*, *4810*, 7 (2002).

[8] Maier, S. A., Brongersma, M. L., Kik, P. G., Meltzer, S., Requicha, A. G., and Atwater, H. A., "Plasmonics - a route to nanoscale optical devices," *Adv. Mater.*, *13(19)*, 1501 (2001).

[9] Maier, S. A., Kik, P. G., and Atwater, H. A., "Optical pulse propagation in metal nanoparticle chain waveguides," *Phys. Rev. B*, *67*, 205402 (2003).

[10] Maier, S. A., Barclay, P. E., Johnson, T. J., Friedman, M. D., and Painter, O., "Low-loss accessible plasmon waveguide for planar energy guiding and sensing," *Appl. Phys. Lett.*, *84*, 3990 (2004).

[11] Ghoshal, A., Webb-Wood, G., Mazuir, C., and Kik, P.G., "Coherent far-field excitation of surface plasmons using resonantly tuned metal nanoparticle arrays," *Proc. SPIE*, *5927(1)* 592714 (2005).

[12] Ozbay, E.,"Plasmonics: merging photonics and electronics at nanoscale dimensions," *Science*, *311*, 189 (2006).

[13] Schaadt, D. M., Feng, B., and Yu, E. T., "Enhanced semiconductor optical absorption vis surface plasmon excitation in metal nanoparticles," *Appl. Phys. Lett.*, *86*, 063106 (2005).

[14] Pillai, S., Catchpole, K. R., Trupke, T., and Green, M. A., "Surface plasmon enhanced silicon solar cells," *J. Appl. Phys.*, *101*, 093105 (2007).

[15] Lim, S. H., Mar, W., Matheu, P., Derkacs, D., and Yu, E. T., "Photocurrent spectroscopy of optical absorption enhancement in silicon photodiodes via scattering from surface plasmon polaritons in gold nanoparticles," *J. Appl. Phys.*, *101*, 104309 (2007).

[16] Derkacs, D., Lim, S. H., Matheu, P.W., Mar, W., and Yu, E. T., "Improved performance of amorphous silicon solar cells via scattering from surface plasmon polaritons in nearby metallic nanoparticles," *Appl. Phys. Lett.*, *89*, 093103 (2006).

[17] Hägglund, C., Zäch, M., Petersson, G., Kasemo, B., "Electromagnetic coupling of light into silicon solar cell by nanodisk plasmons," *Appl. Phys. Lett.*, *92*, 053110 (2008).

[18] Jensen, T. R., Schatz, G. C., and Van Duyne, R. P., "Nanosphere lithography: surface plasmon resonance spectrum of a periodic array of silver nanoparticles by ultraviolet-visible extinction spectroscopy and electrodynamic modeling," *J. Phys. Chem. B*, *103*, 2394 (1999).

[19] Haynes, C. L., McFarland, A. D., Zhao, L., Van Duyne, R. P., and Schatz, G. C., "Nanoparticle optics: the importance of radiative dipole coupling in two-dimensional nanoparticle arrays," *J. Phys. Chem. B*, *107*, 7337 (2003).

[20] Zhao, L., Kelly, K. L., and Schatz, G. C., "The extinction spectra of silver nanoparticle arrays: influence of array structure on plasmon resonance wavelength and width," *J. Phys. Chem. B*, *107*, 7343 (2003).

[21] Zou, S., Janel, N., and Schatz, G. C., "Silver nanoparticle array structures that produce remarkable narrow plasmon lineshapes," *J. Chem. Phys.*, *120*, 10871 (2004).

[22] Chu, T. C., Tsai, D. P., and Liu, W.-C., "Surface plasmon resonance in metallic nanocylinder array," *J. Kor. Phys. Soc.*, *47*, S194 (2005).

[23] Huang, W., Qian, W. and El-Sayed, M. A., "The optically detected coherent lattice oscillations in silver and gold monolayer periodic nanoprism arrays: the effect of interparticle coupling," *J. Phys. Chem. B*, *109*, 18881 (2005).

[24] Hicks, E. M., Zou, S. Z., Schatz, G. C., Spears, K. G., and Van Duyne, R. P., *Nano Lett.*, *5(6)*, 1065 (2005).

[25] Bouhelier, A., Bachelot,R., Im, J.,S., Wiederrecht, G. P., Lerondel, G., Kostcheev, S., Royer,P., "Electromagnetic interactions in plasmonic nanoparticle arrays," *J. Phys. Chem. B*, *109*, 3195 (2005).

[26] Pedersen, D.B., Wang, S. L., Paige, M. F., Leontowich, A. F. G., "Exploiting near-field coupling between closely spaced, gas-phase, 10 +/- 5 nm Ag nanoparticles deposited on NaCl to observe the quadrupolar surface plasmon absorption," *J. Phys. Chem. C*, *111*, 5592 (2007).

[27] Khlebtsov, B. N., Khanadeyev, V. A., Ye, J., Mackowski, D. W., Borghs, G., and Khlebtsov, N. G., "Coupled plasmon resonances in monolayers of metal nanoparticles and nanoshells," *Phys. Rev. B*, *77*, 035440 (2008).

[28] Gantzounis, G., Stefanou, N., and Papanikolaou, N., "Optical properties of periodic structures of metallic nanodisks," *Phys. Rev. B*, *77*, 035101 (2008)

[29] Zheng, Y. B., Juluri, B. K., Mao, X., Walker, T. R., and Huang, T. J., "Systematic investigation of localized surface plasmon resonance of long-range ordered Au nanodisk arrays," *J. Appl. Phys.*, *103*, 014308 (2008).

[30] Utegulov, Z. N., Shaw, J. M., Draine, B. T., Kim, S. A., and Johnson, W. L., "Surface-plasmon enhancement of Brillouin light scattering from gold-nanodisk arrays on glass," *Proc. SPIE*, *6641*, 66411M (2007).

[31] Purcell, E. M., and Pennypacker, C. R., "Scattering and absorption of light by nonspherical dielectric grains [in the interstellar medium]", *Astrophys. J.*, *186(2)*, 705 (1973).

[32] Draine, B. T., and Goodman, J., "Beyond Clausius-Mossotti: wave propagation on a polarizable point lattice and the discrete dipole approximation," *Astrophys. J.*, *405(2)*, 685 (1993).

[33] Draine, B. T., and Flatau, P. J., "Discrete dipole approximation for scattering calculations," *J. Opt. Soc. Am. A*, *11(4)*, 1491 (1994).

[34] DDSCAT can be downloaded from *http://www.astro.princeton.edu/ draine/DDSCAT.html*.

[35] Draine, B. T., and Flatau, P. J., "The discrete dipole approximation for periodic targets: I. Theory and tests," (submitted for publication).

[36] Johnson, P. B., and Christy, R. W., "Optical constants of the noble metals," *Phys. Rev. B*, *6*, 4370 (1972).

[37] Philipp, H. R., "Silicon Nitride (Si_3N_4) (Noncrystalline)," in *Handbook of Optical Constants of Solids* (Academic, 1985), pp. 771-774.

[38] Djurišić, A. B., and Li, E. H., "Modeling the index of refraction of insulating solids with a modified Lorentz oscillator model," *Appl. Optics*, *37(22)*, 5291 (1998).

[39] French, A. P., *Vibrations and Waves* (W. W. Norton, New York, 1971).